sciendo

Civil and Environmental Engineering
Vol. 17, Issue 1, 66-81, DOI: 10.2478/cee-2021-0008

ESTIMATING FLOOD INUNDATION DEPTH ALONG THE ARTERIAL ROAD BASED ON THE RAINFALL INTENSITY

Agus SUHARYANTO[1,*]

[1] Civil Engineering Department, Faculty of Engineering, Universitas Brawijaya, Jl. MT. Haryono 167, Malang 65145, Indonesia.
[*] corresponding author: agus.s@ub.ac.id

Abstract

This study identifies the rainfall intensity that causes the flood along the arterial road connecting Malang to Surabaya, East Java, Indonesia, estimates flood occurrences based on the recorded rainfall data, and proposes the normalization of the side ditch to reduce flood occurrences. The Nakayasu synthetic unit hydrograph was used to analyze the runoff discharge, and the Hydrologic Engineering Center's River Analysis System software was used to analyze the water level profile of the side ditch. The regression method was used to determine the relationship between the rainfall intensity and inundation depth along the arterial road. Analysis results show that floods occur if the rainfall intensity is ≥1.01 year return period. To estimate the flood inundation depth, simple linear regression was conducted herein. Furthermore, it was observed that flood occurrences can be avoided by normalizing the side ditch cross section with a fully rectangular shape having a channel bottom elevation equal to the existing elevation.

Keywords:

Flood inundation;
Arterial road;
Rainfall intensity;
Channel normalization;
Return period.

1 Introduction

The arterial roads are important for the intercity transport of humans and goods. Road problems or accidents occurring on these roads could cause gridlocks. Consequently, the travel time will be delayed, leading to economic losses. Obstacles such as flood inundation also occur along arterial roads. Flood along the arterial road is caused by overflow from the side ditch [1, 2]. To prevent flood occurrences, the rainfall intensity that causes floods must be determined. Moreover, the inundation depth along the arterial road depends on the rainfall intensity in the watershed area. Thus, an early warning system must be developed to minimize economic losses due to the inundation time. This phenomenon has occurred along the arterial road connecting Malang to Surabaya, East Java, Indonesia. Nearly every year, particularly in the rainy season, floods occur approximately 35 km from Malang City of the arterial road connecting Malang to Surabaya, East Java, Indonesia. The most recent flood occurred on January 4, 2019. With a daily traffic volume of approximately 22 000 vehicles, traffic jams occur during floods. The inundation time is approximately 2 h; therefore, traffic jams could last for approximately 2 h. To prevent flood occurrences, the rainfall intensity that causes floods and the relationship between rainfall intensity and inundation depth must be determined. Therefore, this study analyzes the rainfall intensity that causes floods along arterial roads and the relationship between rainfall intensity and inundation depth. To minimize the inundation depth, a suitable increase in the size of the side ditch is proposed. The relationship between rainfall intensity and inundation depth can be either linear or nonlinear.

Generally, a flood occurrence is caused by runoff discharge that is larger than the capacity of the channel [3, 4]. One of the dynamic data that can be used as an input in runoff discharge analysis is the rainfall intensity [5, 6]. That is, the higher the rainfall intensity, the larger the runoff discharge. If the runoff discharge is larger than the capacity of the channel, then an overflow will occur from the lowest channel riverbank. If the channel is a side ditch, the overflow discharge will inundate the road

beside the side ditch. The inundation depth along the road depends on the difference in rainfall intensity received by the channel and the peak of rainfall intensity. To increase the capacity of the channel, normalization or expansion of the size of the channel is necessary. On the basis of the location of the side ditch, the limited size of the side ditch can be normalized. Generally, the normalization of the side ditch depends on the type of road beside the side ditch, cross sectional channel type, and comparison between the depth and width of the channel [7, 8]. The average rainfall intensity in the watershed area will be used as input data in the surface runoff discharge analysis [9-11]. The runoff coefficient will be derived from satellite imagery data [12, 13], and the physical characteristics of the watershed area will be analyzed using the topographic map generated by the geographic information system (GIS) [14, 15]. The surface runoff discharge analysis will be performed using the Nakayasu synthetic unit hydrograph (SUH) [16-18]. The water level analysis of the side ditch will be conducted using the Hydrologic Engineering Center's River Analysis System (HEC-RAS) software.

2 Materials and methods

The research area is located along the arterial road connecting Malang to Surabaya, East Java, Indonesia. Floods occur approximately 35 km from Malang City of the arterial road connecting Malang to Surabaya, East Java, Indonesia. From Malang to Surabaya along the upstream to downstream direction, the side ditch located at the left side of the arterial road is 15 km long. Nearly every year, floods occur approximately 1.5 km from the end of the side ditch. Two sheets of topographic maps scaling 1:25 000 were used to analyze the physical characteristics of the watershed of the side ditch, such as watershed boundary, area, slope, and length of the river [19, 20]. The Landsat 8 Operational Land Imager (OLI) satellite imagery scanned in 2019 was used to generate the land cover to estimate the runoff coefficient [21, 22]. The 11 year daily rainfall data from 2009 to 2019 were used to analyze the average maximum rainfall intensity. Finally, a 1 km long topographic survey was conducted approximately 1 km from the end of the side ditch toward the upstream direction for collecting cross sectional data. Other data, such as materials components of the side ditch to estimate Manning's roughness coefficient, baseflow, and the existing water level of the side ditch, were collected through direct observation in the field.

2.1 Rainfall intensity

On the basis of available data, the average rainfall intensity in the watershed area was analyzed using the maximum daily rainfall intensity for each year. The 11 year data recorded by rainfall stations were used. The Thiessen polygon method was used to determine the average rainfall intensity in the watershed area. Using appropriate statistical characteristics of the average rainfall intensity data distribution, the daily rainfall intensities of multiyear return periods were analyzed [23-26]. The types of rainfall intensity data distribution include normal, log-normal, Gumbel, and log-pearson type III (LP type III) distributions. The parameters used to select the appropriate data distribution type are shown in Table 1. After the determination of daily-rainfall intensities of multiyear return periods, the data were converted into hourly rainfall intensities to analyze the runoff discharge. The analysis was conducted using Mononobe's formula provided in Equation 1 [27, 28]. The hourly rainfall intensity analysis results can be used as input data to analyze the runoff discharge using the Nakayasu SUH.

$$R_t = \frac{R_{24}}{T}\left(\frac{T}{t}\right)^{2/3}, \tag{1}$$

where R_t is the hourly rainfall intensity [mm/h], R_{24} is the daily rainfall intensity [mm/day], T is the rainfall duration (equal to 24 h for daily rainfall), and t is the actual rainfall duration [h].

Table 1: Distribution characteristics.

No.	Types	Prerequisite	Description
1.	Normal	$Cs \approx 0$, $Ck \approx 3$	Cs = Skewness coefficient Ck = Kurtosis coefficient Cv = Variant coefficient
2.	Log Normal	$Cs \approx 3\ Cv + Cv^2 = 3$ $Ck \approx 5.383$	
3.	Gumbel	$Cs \leq 1.1396$, $Ck \leq 5.4002$	
4.	Pearson type III	$Cs \neq 0$, $Cv = 0.3$	
5.	Log-Pearson type III	$Cs < 0$, $Cv = 0.3$	

2.2 Runoff discharge analysis

Surface runoff analysis was performed using the Nakayasu SUH. The formulas of the Nakayasu SUH can be expressed as follows [29].

$$Qp = \frac{C.A.Ro}{3.6(0.3Tp.T0.3)}, \tag{2}$$

$$Qa = Qp\left(\frac{t}{Tp}\right)^{2.4}, \tag{3}$$

$$T_{0.3} = \beta\ tg, \tag{4}$$

$$\beta = \frac{0.47(A.L)^{0.25}}{tg}, \tag{5}$$

$$Tp = tg + 0.8\ tr, \tag{6}$$

if $L < 15$ km, then $tg = 0.21\ L^{0.7}$, (7)

if $L > 15$ km, then $tg = 0.4 + 0.58\ L$, (8)

For $0 \leq t \leq (Tp + T_{0,3})$

$$Qd_1 = Qp.0.3^{\frac{t-Tp}{T_{0.3}}}, \tag{9}$$

For $(Tp + T_{0,3}) \leq t \leq (Tp + T_{0,3} + 1{,}5\ T_{0,3})$

$$Qd_2 = Qp.0.3^{\frac{t-Tp+0.5.T_{0.3}}{1.5.T_{0.3}}}, \tag{10}$$

For $t > (Tp + T_{0,3} + 1{,}5\ T_{0,3})$

$$Qd_3 = Qp.0.3^{\frac{t-Tp+1.5.T_{0.3}}{2.T_{0.3}}}. \tag{11}$$

Here, Qa is the rising-limb discharge [m^3/s]; t is the time [h]; Qp is the peak discharge [m^3/s]; Qd is the falling-limb discharge [m^3/s]; C is the surface runoff coefficient; A is the watershed area [km^2]; R_o is the rainfall unit [mm]; T_p is the time to peak [h], which is the time from the start of rainfall to the peak discharge; $T_{0.3}$ is the time required to subside from the maximum peak discharge to 30 % of the peak discharge; L is the channel length [km]; tg is the lag time [h]; tr is 0.5tg to tg [h] that depends on the rainfall data interval flood unit time [h]; and β is the hydrograph parameter. The typical Nakayasu SUH is illustrated in Fig. 1.

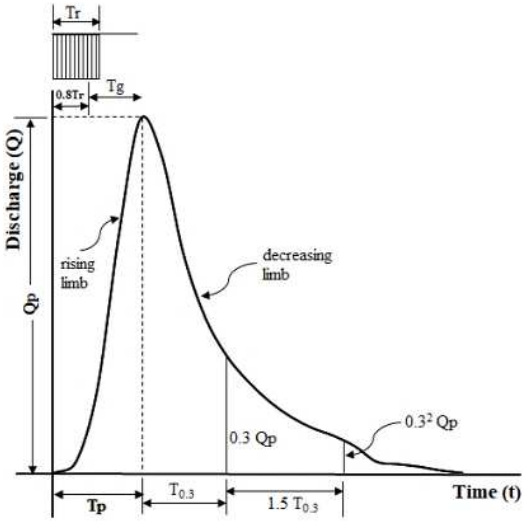


Fig. 1: Schematic of the Nakayasu SUH.

To implement the Nakayasu SUH, *A* and *L* were analyzed using the topographic map generated by the GIS [14, 15]. *C* was estimated on the basis of the land cover map generated from Landsat 8 satellite imagery and combined with the different values of *C* shown in Table 2 [21, 22]. The weighted average method was used to analyze the average *C* in the watershed.

The unsupervised classification method was used to classify the land cover map from the satellite imagery [30, 31]. The ER Mapper image analysis software was used for the land cover analysis. Surface runoff analysis was conducted using the Nakayasu SUH by inputting the hourly rainfall intensity of multiyear return periods and other required data. Finally, the surface runoff discharge from the watershed in multiyear return periods was determined.

2.3 Water level analysis

To analyze the water level of the side ditch, the standard step method was applied. The basic equations can be expressed as follows [32, 33]:

$$Y_2 + Z_2 + \frac{\alpha_2 V_2^2}{2g} = Y_1 + Z_1 + \frac{\alpha_1 V_1^2}{2g} + he\,, \tag{12}$$

$$he = L.S_f + Co\left|\frac{\alpha_2 V_2^2}{2g} - \frac{\alpha_1 V_1^2}{2g}\right|, \tag{13}$$

where Y_1 and Y_2 are the water depths [m]; Z_1 and Z_2 are the channel bottom elevations [m]; V_1 and V_2 are the velocities [m/s]; α_1 and α_2 are the coefficients; g is the gravitational acceleration [m^2/s]; he is the energy loss [m]; L is the river length [m]; and Co is the coefficient of energy loss caused by the cross sectional change. To analyze the water level of the channel, the HEC-RAS software was used. Cross sectional data were collected by conducting a topographical survey. Flood occurrences were analyzed by determining the water level and riverbank elevation of each channel cross section. The flood occurrence can be predicted if the water level is higher than the riverbank elevation. The inundation depth was calculated as the difference between the water level and arterial road elevation.

Table 2: Runoff coefficients.

Land cover	*C*	Land cover	*C*
Business		**Lawns, sandy soil**	
Downtown	0.70 – 0.95	Flat, 2 %	0.05 – 0.1
Neighborhood	0.50 – 0.70	Average, 2 % –7 %	0.1 – 0.15
Residential		Steep, > 7 %	0.15 – 0.20
Single-family	0.30 – 0.50	**Lawns, heavy soil**	
Multiunits, detached	0.40 – 0.60	Flat, 2 %	0.17 – 0.17
Multiunits, attached	0.60 – 0.75	Average, 2 % – 7 %	0.18 – 0.22
Residential (suburban)	0.25 – 0.4	Steep, > 7 %	0.25 – 0.35
Industrial		**Agricultural area**	
Light	0.50 – 0.80	Open land	
Heavy	0.60 – 0.90	Flat	0.30 – 0.60
Parks, cemeteries	0.10 – 0.25	Rough	0.20 – 0.50
Playground	0.20 – 0.35	**Cultivated area**	
Railroad yard	0.20 – 0.35	Heavy soil, no vegetation	0.30 – 0.60
Unimproved	0.10 – 0.30	Heavy soil, vegetation	0.20 – 0.50
Pavements		Sandy soil, no vegetation	0.20 – 0.25
Asphalt	0.70 – 0.85	Sandy soil, vegetation	0.10 – 0.25
Concrete	0.70 – 0.95	**Meadow**	
Stone/brick	0.70 – 0.85	Heavy soil	0.15 – 0.45
Pedestrian	0.75 – 0.85	Sandy soil	0.05 – 0.25
Roofs	0.75 – 0.95	Forest, vegetation	0.05 – 0.25
		Bare land	
		Flat, impervious	0.70 – 0.90
		Rough	0.50 – 0.70

Source: [34]

To minimize flood occurrences, the dimensions of the side ditch cross section were normalized to achieve the ideal cross section, such as trapezoidal or rectangular shapes. Owing to the limited land boundaries of the left and right banks, normalization can only be performed by increasing the side ditch depth. The right side of the side ditch is the arterial road, and the left side of the side ditch is the residential area. A threshold for the increase in the side ditch depth ensures the best performance of the side ditch in transporting runoff discharge.

2.4 Relationship between rainfall intensity and inundation depth

Analysis results reveal the relationship between the rainfall intensity and inundation depth at the pavement area of the arterial road. The simulation is conducted by inputting the rainfall intensity data of the 1.01, 2, 5, 10, 25, and 50 year return periods. Furthermore, the analysis results present the inundation depth along the arterial road. A graph showing the regression results of the relationship between the rainfall intensity and inundation depth reveals that the inundation depth along the arterial road can be estimated on the basis of the rainfall intensity. Finally, this graph can be used as a reference for the early warning system for predicting flood occurrences and traffic jams along arterial roads.

3 Results and discussions

The watershed of the side ditch was analyzed using the ArcMap 10.6 GIS software. The river network was generated from the topographic map. The watershed boundary was analyzed by overlapping the river network and digital elevation model. The analysis results show that the watershed area, that is, the Purwodadi watershed, is equal to 80.764 km^2. The Purwodadi watershed has 16 subwatersheds and 9 lateral flow areas. The location and shape of the Purwodadi watershed

are shown in Fig. 2. The longest and shortest river lengths are 0.133 and 17.355 km, respectively. The topographic map of the watershed is shown in Fig. 3. The highest and lowest elevations of the Purwodadi watershed are 3 230 and 250 m, respectively. The physical data of the Purwodadi watershed are summarized in Table 3.

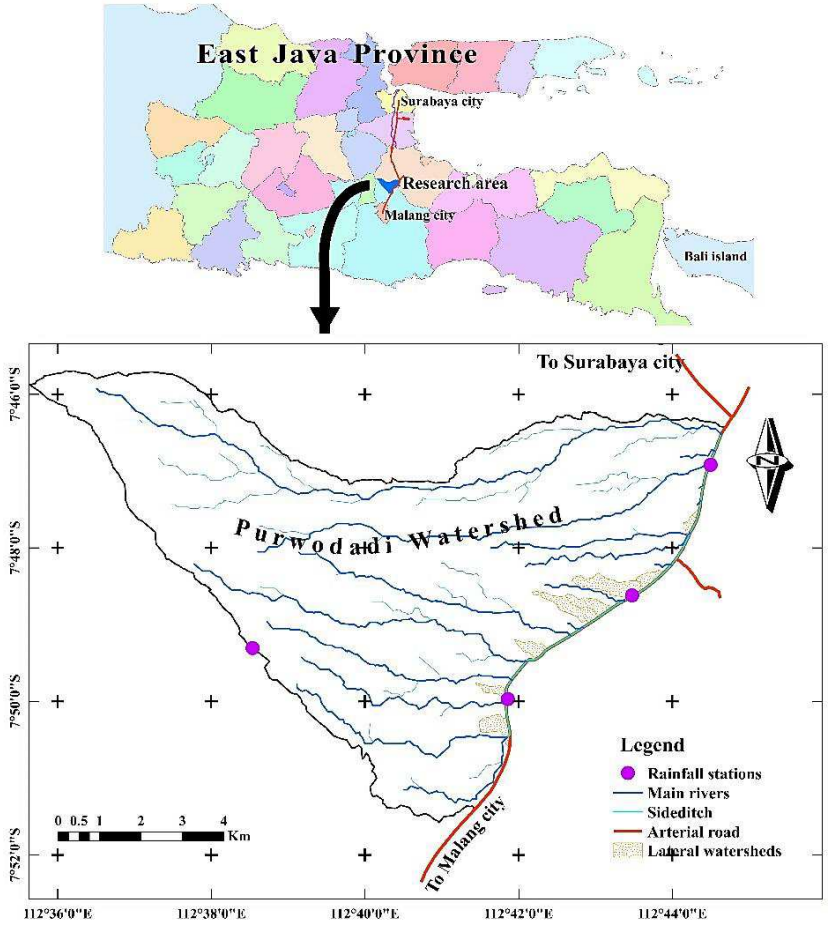


Fig. 2: Purwodadi watershed.

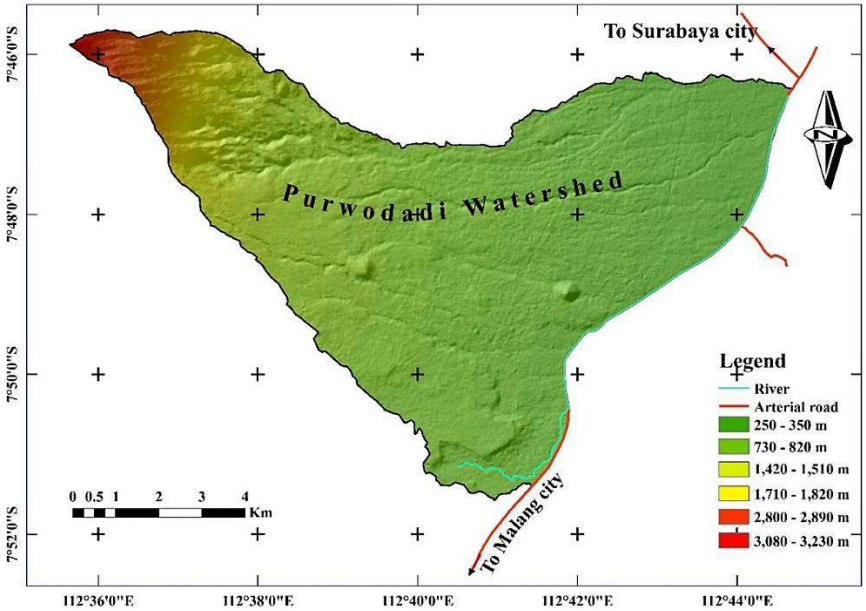


Fig. 3: Topographic map of the Purwodadi watershed.

Table 3: Physical characteristics of the Purwodadi watershed.

No.	Sub-watersheds	Length of the river [km]	Area [km^2]
1.	Subwatershed 1	17.355	25.803
2.	Subwatershed 2	0.973	0.845
3.	Subwatershed 3	12.154	10.133
4.	Subwatershed 4	0.149	0.495
5.	Subwatershed 5	0.133	0.570
6.	Subwatershed 6	5.074	2.854
7.	Subwatershed 7	4.758	2.406
8.	Subwatershed 8	0.435	0.706
9.	Subwatershed 9	2.115	1.169
10.	Subwatershed 10	0.422	0.674
11.	Subwatershed 11	7.472	7.205
12.	Subwatershed 12	9.401	7.662
13.	Subwatershed 13	6.674	5.805
14.	Subwatershed 14	6.040	3.605
15.	Subwatershed 15	6.436	4.751
16.	Subwatershed 16	3.849	4.172
17.	Lateral flow 1		0.019
18.	Lateral flow 2		0.084
19.	Lateral flow 3		0.151
20.	Lateral flow 4		0.466
21.	Lateral flow 5		0.243
22.	Lateral flow 6		0.364
23.	Lateral flow 7		0.177
24.	Lateral flow 8		0.113
25.	Lateral flow 9		0.292
Total area			80.746

3.1 Rainfall intensity during multiyear return periods

The Purwodadi watershed has four rainfall stations, namely, Purwosari, Purwodadi, Lawang, and Kebun Teh rainfall stations. The maximum daily-rainfall intensity from 1999 to 2019 was selected from these rainfall stations. The average rainfall intensity in the watershed area was analyzed using the Thiessen polygon shown in Fig. 4. Table 4 shows the average rainfall intensity in the Purwodadi watershed. The distribution type of these data was analyzed using the statistical analysis and parameter criteria shown in Table 1. The LP type III was the most appropriate distribution type of these data. Consequently, the rainfall intensities of the 1.01, 2, 5, 10, 25, and 50 year return periods were calculated using the LP type III formula. The daily-rainfall data were converted into hourly rainfall data using Equation 1 with the assumption that the rainfall duration is equal to 4 h. The daily and hourly rainfall data of the multiyear return periods are shown in Table 5.

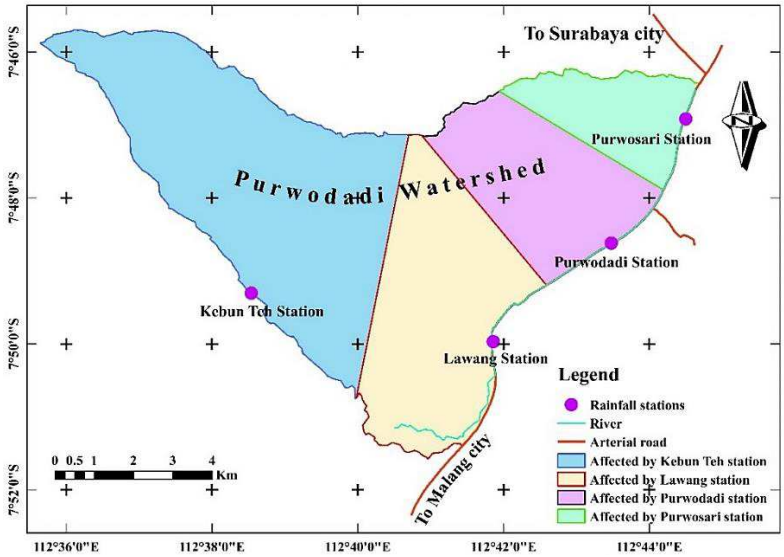


Fig. 4: Rainfall stations and Thiessen polygon.

Table 4: Average rainfall intensity in the Purwodadi watershed.

No.	Year	Maximum rainfall intensity [mm/day]				
		Purwosari	Purwodadi	Lawang	Kebun Teh	Average
1.	2009	76	98	46	85	75.952
2.	2010	125	130	48	105	96.192
3.	2011	90	98	64	99	88.468
4.	2012	75	106	144	77	100.197
5.	2013	105	115	117	87	102.027
6.	2014	80	120	108	102	104.715
7.	2015	135	165	114	94	116.503
8.	2016	140	94	75	114	102.411
9.	2017	132	127	102	125	119.858
10.	2018	118	95	81	91	91.735
11.	2019	75	138	125	82	103.162

Table 5: Rainfall intensity of the multiyear return periods.

No.	Return periods [year]	Daily [mm/day]	Hourly [mm/h]			
			1	2	3	4
1.	1.01	65.33	10.70	41.16	7.50	5.97
2.	2	96.89	15.86	61.04	11.13	8.86
3.	5	106.91	17.51	67.35	12.28	9.78
4.	10	111.62	18.28	70.32	12.82	10.21
5.	25	113.37	18.56	71.42	13.02	10.37
6.	50	118.88	19.47	74.89	13.65	10.87

3.2 Runoff coefficient

Landsat 8 OLI imagery scanned on October 18, 2019 was used to classify the land cover at the Purwodadi watershed. Unsupervised classification method was used, and seven categories of land cover types were classified. Fig. 5 shows the land cover of the Purwodadi watershed. The land cover types and area of each type are shown in Table 6. Based on the land cover type area and *C* value, as shown in Table 2, the *C* value, which was obtained using the weighted average method, of the Purwodadi watershed was found to be 0.55.

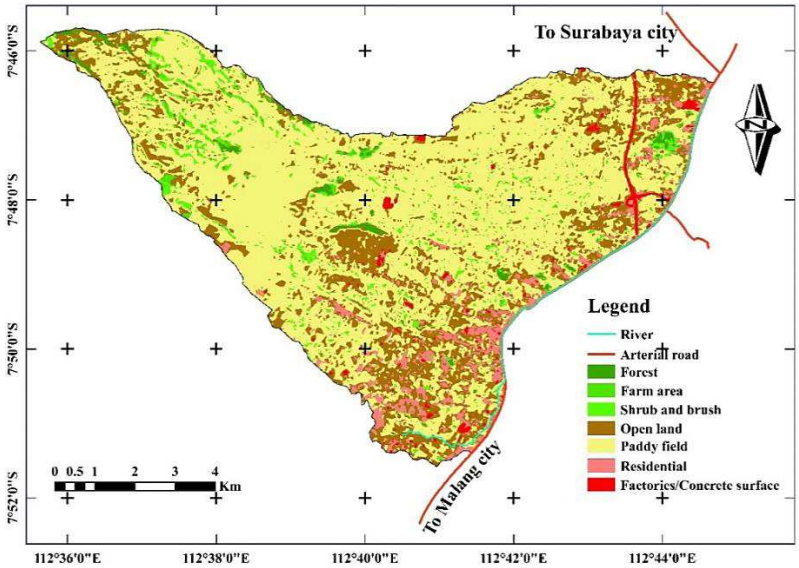


Fig. 5: Land cover types at the Purwodadi watershed.

Table 6: Land cover types at the Purwodadi watershed.

No.	Land cover categories	Area [km^2]
1.	Forest	0.737
2.	Farm area	0.544
3.	Shrub and Brush	3.640
4.	Open land	16.383
5.	Paddy field	54.173
6.	Residential	4.139
7.	Factories/Concrete surface	1.140
Total area		80.756

3.3 Cross sectional data

The total length of the side ditch of the Purwodadi watershed is approximately 15 km. Along the side ditch, the flood only occurred at a distance of approximately 1 km. Therefore, the side ditch wherein floods often occurred was selected as the research area herein. The cross sectional data along 1 km of the research area was topographically surveyed with an interval of 50 m. The cross sections were numbered from 1 to 21 from the downstream to upstream direction.

3.4 Runoff discharge and inundation depth of the multiyear return periods

On the basis of the data shown in Tables 3, 5, and 6, the runoff discharge of multiyear return periods was analyzed using the Nakayasu SUH. The hydrograph of the analysis results is shown in Fig. 6. The time to peak and peak discharge for each year's return period is shown in Table 7. Based on the runoff discharge data, the water level of the Purwodadi arterial road, particularly the side ditch, was analyzed using the HEC-RAS software. A part of the analysis results, that is, the water level at cross section no. 15 or station no. 0+700, is shown in Fig. 7. The analysis was conducted by inputting the 1.01 year return period runoff discharge. With the same runoff discharge, the longitudinal water level profile along 1 km of the side ditch is shown in Fig. 8.

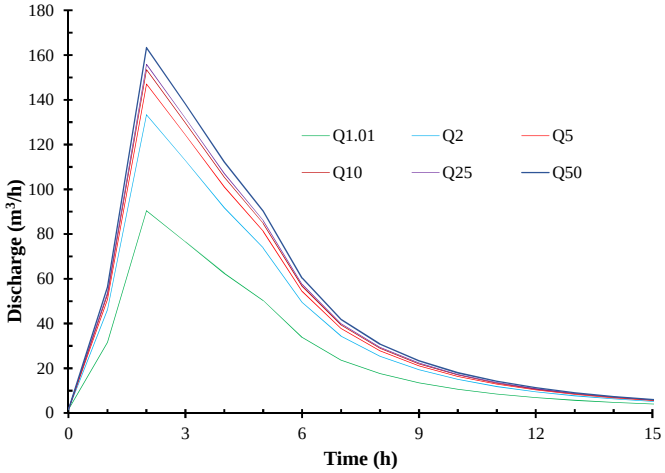


Fig. 6: Nakayasu SUH at the Purwodadi watershed.

Table 7: Time to peak and peak discharge.

No.	Return periods [year]	*Tp* [h]	*Qp* [mm/h]
1.	1.01	1.635	90.443
2.	2	1.635	133.395
3.	5	1.635	147.031
4.	10	1.635	153.437
5.	25	1.635	155.818
6.	50	1.635	163.321

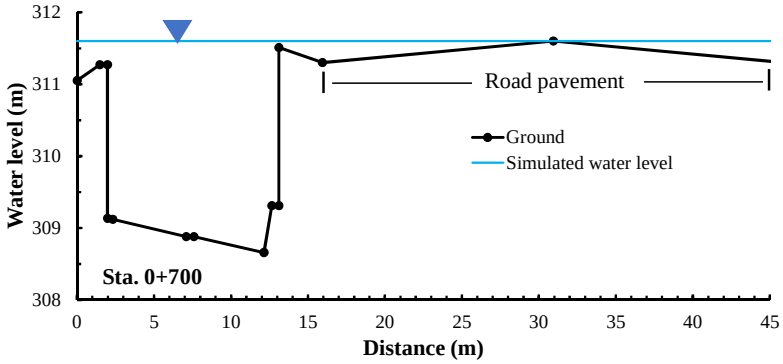


Fig. 7: Water level profile of the side ditch cross section No. 15.

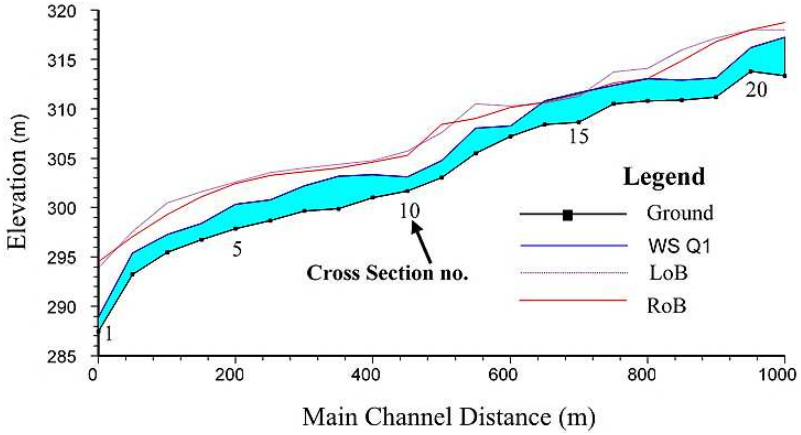


Fig. 8: Longitudinal water level profile of the side ditch.

Analysis results show that not all subwatersheds of the Purwodadi watershed contributed to the discharge along the surveyed side ditch of the arterial road. Subwatershed no. 1, 2, and 3 did not

contribute to the discharge at the watershed of the side ditch. Consequently, the watershed area analyzed herein is equal to 43.965 km^2. Using *A*, *C*, *R*, runoff discharge of the 1.01 year return period (Q1), and the surveyed side ditch cross section as the main input data, the water level of the side ditch was analyzed using the HEC-RAS software. Analysis results show that overflow occurred at cross section no. 15 or station no. 0+700. The elevation of the right side of the riverbank was equal to 311.510 m, and the water level was equal to 311.602 m. Therefore, an overflow occurred at station no. 0+700, with a depth of 9 cm from the riverbank. Herein, the inundation depth was measured on the basis of the elevation along the arterial road berm. At cross section no. 15, the berm elevation was equal to 311.602 m. Consequently, the inundation depth at station no. 0+700 was equal to 30.2 cm (311.602–311.300 m). Similarly, the water level of the side ditch was analyzed using the runoff discharge of the 2 (Q2), 5 (Q5), 10 (Q10), 25 (Q25), and 50 (Q50) year return periods. Analysis results show that overflow occurred in many cross sections. At Q2, overflow occurred at cross section no. 14, 15, 16, and 17 or station no. 0+650, 0+700, 0+750, and 0+800, with inundation depths equal to 48.6, 84.0, 28.3, and 37.0 cm, respectively. In the same cases, overflow occurred in five cross sections (no. 8, 14, 15, 16, and 17) for Q5, Q10, Q25, and Q50 as input data. In summary, the inundation depths of the side ditch due to the runoff discharge at Q1–Q50 are shown in Table 8. Based on the data shown in this table, the relationship between rainfall intensity and inundation depth in station no. 15 at Q1–Q50 are illustrated in Fig. 9. Fig. 9 shows that the relationship is linear with the following regression equation:

$$Y = 1.6544X - 77.313, \text{ with } R^2 \text{ equal to } 0.9994. \quad (14)$$

For the floods that occurred on January 5, 2017, and January 4, 2019, the inundation depths estimated from Figs. 10 and 11 are approximately equal to 80 and 70 cm, respectively. The location is approximately 10 m from station no. 15. The recorded daily-rainfall intensities are equal to 104, 127, 44, and 110 mm (Fig. 10) and 51, 22, 125, and 105 mm (Fig. 11) for the Purwosari, Purwodadi, Lawang, and Kebun Teh rainfall stations, respectively. The average daily-rainfall intensities are equal to 94.7 and 89.8 cm. Using the graph shown in Fig. 9, the inundation depths are estimated to be equal to 79.5 and 71.4 cm. These values are consistent with the inundation depths estimated from the inundation depths shown in Figs. 10 and 11. Therefore, the graph shown in Fig. 9 can be used to estimate the flood inundation at the side ditch based on the rainfall intensity recorded at the Purwosari, Purwodadi, Lawang, and Kebun Teh rainfall stations.

To minimize flood occurrences, watershed management, channel normalization, and floodways must be implemented. Based on the physical conditions at the Purwodadi watershed and those of the side ditch, channel normalization is the most appropriate method to minimize flood occurrences because the channel is relatively short (approximately 15 km long) and its sole function is to protect arterial roads from floods. The side ditch cross section is changed from its existing condition to a fully rectangular cross section with a bottom elevation that is equal to the lowest existing bottom elevation. The normalized cross section no. 15 is shown in Fig. 12. The water level of the side ditch with runoff discharge at Q1 to Q50 was simulated. Results are summarized in Table 9. This table shows that floods occurred at cross section no. 15 with runoff discharge of 2, 5, 10, 25, and 50 year return periods. The inundation depths of these return periods are 11.5, 11.6, 11.8, 13.7, and 15.5 cm. Thus, the average flood inundation depth is only approximately 12 cm. Therefore, by the normalization of the side ditch cross section, floods along the arterial road connecting Malang to Surabaya, East Java, Indonesia, can be minimized.

Table 8: Inundation depths.

Return period [year]	Simulated water level [m]	Berm elevation [m]	Inundation depth [m]	Over flow
Cross section no. 8 (0+350)				
1.01	303.210	304.110	−0.900	No
2	304.090	304.110	−0.020	No
5	304.340	304.110	0.230	Yes
10	304.460	304.110	0.350	Yes
25	304.510	304.110	0.400	Yes
50	304.690	304.110	0.580	Yes
Cross section no. 14 (0+650)				
1.01	310.792	310.820	−0.028	No
2	311.306	310.820	0.486	Yes
5	311.431	310.820	0.611	Yes
10	311.491	310.820	0.671	Yes
25	311.512	310.820	0.692	Yes
50	311.606	310.820	0.786	Yes
Cross section no. 15 (0+700)				
1.01	311.602	311.300	0.302	Yes
2	312.140	311.300	0.840	Yes
5	312.302	311.300	1.002	Yes
10	312.375	311.300	1.075	Yes
25	312.402	311.300	1.102	Yes
50	312.482	311.300	1.182	Yes
Cross section no. 16 (0+750)				
1.01	312.373	312.610	−0.237	No
2	312.893	312.610	0.283	Yes
5	313.032	312.610	0.422	Yes
10	313.092	312.610	0.482	Yes
25	313.113	312.610	0.503	Yes
50	313.283	312.610	0.673	Yes
Cross section no. 17 (0+800)				
1.01	313.070	313.210	−0.140	No
2	313.580	313.210	0.370	Yes
5	313.730	313.210	0.520	Yes
10	313.800	313.210	0.590	Yes
25	313.820	313.210	0.610	Yes
50	313.962	313.210	0.673	Yes

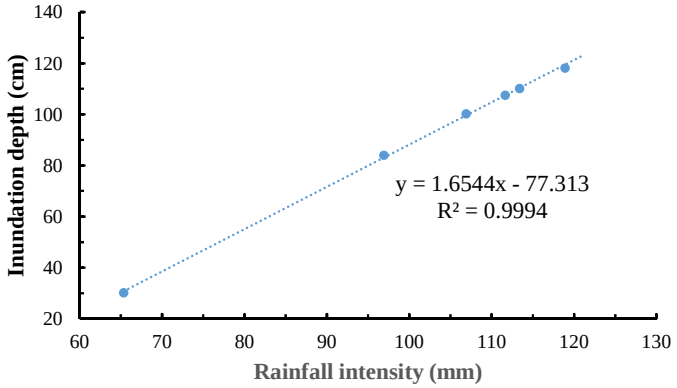


Fig. 9: Relationship between the rainfall intensity and inundation depth.



Fig. 10: Flood that occurred on January 5, 2017 (from the upstream side).



Fig. 11: Flood on January 4, 2019.

To anticipate flood occurrences, an automatic rainfall recorder (ARR) must be established at the Purwosari, Purwodadi, Lawang, and Kebun Teh rainfall stations. If the rainfall intensity can be recorded using the ARR, then the hourly rainfall intensity can be directly recorded. Therefore, from the data shown in Fig. 9, flood occurrences can be predicted. If rainfalls have a duration of more than 4 h with an intensity of more than 10.70, 41.16, 7.50, and 5.97 mm (as shown in Table 5), then floods will occur with inundation depths of more than 30 cm (as shown in Table 8). If the rainfall duration is 2 h, then floods will occur with the hourly rainfall intensities greater than 74.01 and 19.24 mm. To estimate the inundation depth based on the rainfall intensity, interpolation based on the data shown in Fig. 9 can be performed. Using the graph shown in Fig. 9, the recorded hourly rainfall intensity can be converted into the daily-rainfall intensity. Based on the estimated inundation depths, obstacles along the arterial road owing to flood inundation can be anticipated. Therefore, the graph shown in Fig. 9 can be used as a reference for the early warning system predicting flood occurrences along the arterial road connecting Malang to Surabaya, East Java, Indonesia. The validity of the graph can be confirmed using the data of the floods that occurred on January 5, 2017, and January 4, 2019, as described previously.

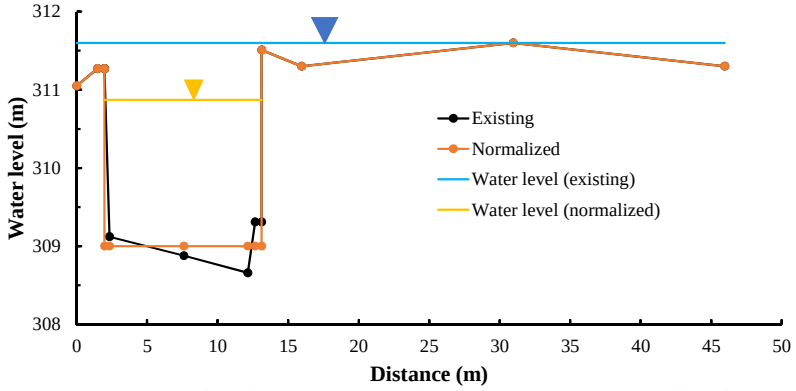


Fig. 12: Water level at cross section no. 15 after normalization.

Table 9: Inundation depths after normalization.

Return period [yr]	Simulated water level [m]	Berm elevation [m]	Inundation depth [m]	Over flow
Cross section no. 15 (0+700)				
1.01	312.040	312.600	−0.560	No
2	312.715	312.600	0.115	Yes
5	312.716	312.600	0.116	Yes
10	312.718	312.600	0.118	Yes
25	312.737	312.600	0.137	Yes
50	312.745	312.600	0.155	Yes

4 Conclusions

This study evidenced that the floods that occurred at the side ditch located approximately 35 km from Malang City of the arterial road connecting Malang to Surabaya, East Java, Indonesia, are caused by rainfall intensities greater than 65.33 mm/day. The graph illustrating the relationship between the rainfall intensity and inundation depth can be used to estimate the flood inundation depth based on the rainfall intensity. Furthermore, it was reported that ARRs must be established at the rainfall stations in the Purwodadi watershed to record the hourly rainfall intensity data. Finally, flood occurrences can be avoided by normalizing the existing side ditch cross sectional shape to a rectangular shape exhibiting a bottom elevation that is similar to the existing bottom elevation.

Acknowledgments

This research was supported by the Water Resources Research Group in the Civil Engineering Department at Universitas Brawijaya Indonesia. The author would like to thank the Faculty of Engineering for supporting this research's budget through the BPPM Program 2019.

References

[1] SHASTRY, A. – DURAND, M.: Utilizing flood inundation observations to obtain floodplain topography in data-scarce regions. Front. Earth Sci., Vol. 6, Iss. 243, 2019, pp. 1-10. doi: 10.3389/feart. 2018. 00243.

[2] VOJTEK, M. – PETROSELLI, A. – VOJTEKOVÁ, J. – ASGHARINIA, S.: Flood inundation mapping in small and ungauged basins: sensitivity analysis using the EBA4SUB and HEC-RAS modeling approach. Hydrology Research, Vol. 50, Iss. 4, 2019, pp.1002-1019. IWA Publishing, doi: 10.2166/nh.2019.163.

[3] SLATER, L. J. – KHOUAKHI, A. – WILBY, R. L.: River channel conveyance capacity adjusts to modes of climate variability. Scientific Reports, Vol. 9, Iss. 12619, 2019, pp. 1-10. Nature research, doi.org/10.1038/s41598-019-48782-1.

[4] CZUBA, J. A. – CZUBA, C. R. – MAGIRL, C. S. – VOSS, F. D.: Channel-conveyance capacity, channel change, and sediment transport in the lower Puyallup, White, and Carbon Rivers. Western Washington, Scientific Investigations Report, Iss. 5240, 2010, pp. 11-19. USGS.

[5] JARA, M. C. – ECHAVEGUREN, T. – BAECHELER, J.V. – GINÉ, A. C. – TAMPIER, H. S.: Reliability-based estimation of traffic interruption probability due to road waterlogging. Journal of Advanced Transportation, Vol. 2018, 2018, pp. 1-12. Hindawi. doi.org/10.1155/2018/2850546.

[6] WANG, W. – YANG, S. – STANLEY, H. E. – GAO, J.: Local floods induce large-scale abrupt failures of road networks. Nature Communications, Vol. 10, Iss. 2114, 2019, pp. 1-11. doi.org/10.1038/s41467-019-10063-w.

[7] MAHMOUDI, M. – TABATABAI, M. R. M. – MOUSAVI, S.: An Analytical Approach to Estimate Optimum River Channel Dimensions. International Journal of Science and Technology, Scientia Iranica, Vol. 26, Iss. 3, 2018, pp. 1169-1181. doi: 10.24200/sci.2018.20552.

[8] NIAZKAR, M. – AFZALI, S. H.: Optimum Design of Lined Channel Sections. Water Resources Management, Vol. 29, Iss. 6, 2015, pp. 1921-1932. doi: 10.1007/s11269-015-0919-9.

[9] RAO, K. N.: Analysis of surface runoff potential in ungauged basin using basin parameters and SCS‑CN method. Applied Water Science, Vol. 10, Iss. 47, 2020, pp. 1-16. doi.org/10.1007/s13201-019-1129-z.

[10] LIU, Z. – CAI, Y. – WANG, S. – LAN, F. – WU, X.: Small and medium-scale river flood controls in highly urbanized areas: a whole region perspective. Water, Vol. 12, Iss. 1, 2020, p. 182. MDPI. doi:10.3390/w12010182.
[11] SAMPAIO, F. E. O. V. – ALVES**,** C. M. A**.:** A procedure to analyze the viability of rainwater harvesting systems in urban areas based on pre-defined diagrams. Brazilian Journal of Water Resources, RBRH, Porto Alegre, Vol. 22, Iss. 60, 2017, pp.10-20. doi.org/10.1590/2318-0331.0217160012.
[12] MAHMOUD, S. H. – MOHAMMAD, F. S. – ALAZBA, A. A.: Determination of potential runoff coefficient for Al-Baha region, Saudi Arabia using GIS. Arab J Geosciences, Vol. 7, 2014, pp. 2041–2057. doi: 10.1007/s12517-014-1303-4.
[13] MUSTAFA, A. – SZYDŁOWSKI, M.: The Impact of spatiotemporal changes in land development (1984–2019) on the increase in the runoff coefficient in Erbil, Kurdistan Region of Iraq. Remote Sensing. Vol. 12, Iss. 8, 2020, p. 1302. MDPI. doi:10.3390/rs12081302.
[14] JUODKIENĖ, V.: GIS in tourism development using spatial modeling. Civil and Environmental Engineering, Vol. 10, Iss. 2, 2014, pp. 98-104. De Gruyter. doi: 10.2478/cee-2014-0018.
[15] WAIYASUSRI, K. – CHOTPANTARAT, S.: Watershed prioritization of Kaeng Lawa sub-watershed, Khon Kaen Province using the morphometric and land-use analysis: a case study of heavy flooding caused by tropical storm Podul. Water, Vol. 12, Iss. 6, 2020, p. 1570. MDPI. doi:10.3390/w12061570.
[16] NATAKUSUMAH, D. K. – HARLAN, D. – HATMOKO, W.: A new synthetic unit hydrograph computation method based on the mass conservation principle. WIT Transactions on Ecology and The Environment, Vol. 172, 2013. WIT Press. doi:10.2495/RBM130031.
[17] TUNAS, I. G. – ANWAR, N. – LASMINTO, U.: Parameters Estimation of Synthetic Unit Hydrograph Model Using Multiple Linear and Non-linear Regressions. 2nd International Conference on Applied Mathematics, 2017. Simulation and Modelling (AMSM). ISBN: 978-1-60595-480-6.
[18] NIGUSSIE, T. A. – YEĞEN, E. B. – MELESSE, A. M.: Performance evaluation of synthetic unit hydrograph methods in Mediterranean climate. A case Study at Guvenc micro-watershed, Turkey, Landscape Dynamics, Soils and Hydrological Processes in Varied Climates, Book Series: Springer Geography, Publisher: Springer International Publishing, 2018, ISBN 978-3-319-18787-7.
[19] SINGH, P – GUPTA, A. – SINGH, M.: Hydrological inferences from watershed analysis for water resource management using remote sensing and GIS techniques. The Egyptian Journal of Remote Sensing and Space Sciences, Vol. 17, Iss. 2, 2014, pp. 111–121. dx.doi.org/10.1016/j.ejrs.2014.09.003.
[20] GEBRE, T. – KIBRU, T. – TESFAYE, S. – TAYE, G.: Analysis of watershed attributes for water resources management using GIS: the case of Chelekot micro-watershed, Tigray, Ethiopia. Journal of Geographic Information System, Vol. 7, Iss. 2, 2015, pp. 177-190. dx.doi.org/ 10.4236/jgis.2015.72015.
[21] HU, S. – FAN, Y. – ZHANG, T.: Assessing the effect of land use change on surface runoff in a rapidly urbanized city: a case study of the central area of Beijing. Land, Vol. 9, Iss. 1, 2020, p. 17. MDPI, doi: 10.3390/land9010017.
[22] SRIWONGSITANON, N. – TAESOMBAT, W.: Effects of land cover on runoff coefficient. Journal of Hydrology, Vol. 410, Iss. 3-4, 2011, pp. 226-238. doi: 10.1016/j.jhydrol.2011.09.021.
[23] KUMAR, R. – BHARDWAJ, A.: Probability analysis of return period of daily maximum rainfall in annual data set of Ludhiana, Punjab. Indian J. Agric. Res., Vol. 49, Iss. 2, 2015, pp. 160-164. Online ISSN: 0976-058X.
[24] BESKOWA, S – CALDEIRAB, T. L. – MELLOC, C. R. – FARIAA, L. C. – GUEDES, H. A. S.: Multiparameter probability distributions for heavy rainfall modeling in extreme southern Brazil. Journal of Hydrology: Regional Studies Vol. 4, Iss. B, 2015, pp. 123-133. dx.doi.org/10.1016/ j.ejrh.2015.06.007.
[25] YE, L. – HANSON, L. S. – DING, P. – WANG, D. – VOGEL, R. M.: The probability distribution of daily precipitation at the point and catchment scales in the United States. Hydrol. Earth Syst. Sci., Vol. 22, Iss. 12, 2018, pp. 6519-6531. doi.org/10.5194/hess-22-6519-2018.
[26] CLARKE, R. T.: Stochastic Hydrology Revisited, RBRH - Revista Brasileira de Recursos Hídricos, Vol. 7, Iss. 4, 2002, pp. 97-104.
[27] KANG, M. S. – GOO, J. H. – SONG, I. – CHUN, J. A. – HER, Y. G. – HWANG, S. W. – PARK, S. W.: Estimating design floods based on the critical storm duration for small watersheds. Journal of Hydro-environment Research. Vol. 7, Iss. 3, 2013, pp. 209-218. 209e218. dx.doi.org/10.1016/j.jher. 2013.01.003.

[28] YOO, C. – JUN, C. – PARK, C.: Effect of rainfall temporal distribution on the conversion factor to convert the fixed-interval into true-interval rainfall. Journal of Hydrologic Engineering, Vol. 20, Iss. 10, 2015. ASCE, doi.org/10.1061/(ASCE)HE.1943-5584.0001178.
[29] KUSUMASTUTI, C. – SUDJARWO, P. – CHRISTHIE, M. – KRISNA, T.: Intensity-duration-frequency (IDF) curve and the most suitable method to determine flood peak discharge in upper Werba sub-watershed. Civil Engineering Dimension, Vol. 21, Iss. 2, 2019, pp. 70-75. doi: 10.9744/CED.21.2.70-75.
[30] GAŠPAROVIĆA, M. – ZRINJSKIB, M. – GUDELJ, M.: Automatic cost-effective method for land cover classification (ALCC). Computers, Environment and Urban Systems, Vol. 76, 2019, pp. 1–10. doi.org/10.1016/j.compenvurbsys.2019.03.001.
[31] VIVEKANANDA, G. N. – SWATHI, R. – SUJITH, A. V. L. N.: Multi-temporal image analysis for LULC classification and change detection. European Journal of Remote Sensing, Vol. 53, Iss. 1, 2020, pp. 1-11. doi:10.1080/22797254.2020.1771215.
[32] SARCHANI, S. – SEIRADAKIS, K. – COULIBALY, P. – TSANIS, I.: Flood inundation mapping in an ungauged basin. Water, Vol. 12, Iss. 6, 2020, p. 1532. MDPI. doi: 10.3390/w12061532.
[33] MOKHTAR, E. S. – PRADHAN, B. – GHAZALI, A. H. – SHAFRI, H. Z. M.: Assessing flood inundation mapping through estimated discharge using GIS and HEC-RAS model. Arabian Journal of Geosciences, Vol. 11, Iss. 682, 2018, pp. 1-20. doi.org/10.1007/s12517-018-4040-2.
[34] ASDAK, C.: Hydrology for watershed management, 5th edition, 2010, pp. 30-50. Gadjah Mada University Press Yogyakarta, Indonesia.